




Dielectric relaxation in layer-structured $\text{SrBi}_{2-x}\text{Gd}_x\text{Nb}_2\text{O}_9$ ($x = 0.0, 0.4, 0.6,$ and 0.8) lead-free ceramics

S. Nagamani¹, J. Nitchal Kiran^{1,*} , B. Siva Basivi Reddy², B. Nageswara Rao¹, J. Anindhya Kiran³, and K. Sambasiva Rao⁴

¹Division of Physics, Department of Sciences & Humanities, VFSTR Deemed to be University, Guntur 522213, India

²Department of Mechanical Engineering, KHIT, Guntur 522019, India

³Department of BS&H, VITS, Deshmukhi, Hyderabad 508284, India

⁴Department of Physics, Andhra University, Visakhapatnam 530003, India

Received: 11 September 2021

Accepted: 10 April 2022

Published online:

28 April 2022

© The Author(s), under exclusive licence to Springer Science+Business Media, LLC, part of Springer Nature 2022

ABSTRACT

The gadolinium (Gd^{3+})-doped $\text{SrBi}_2\text{Nb}_2\text{O}_9$ (SBN) ceramics with the chemical formula $\text{SrBi}_{2-x}\text{Gd}_x\text{Nb}_2\text{O}_9$ ($x = 0.0, 0.4, 0.6,$ and 0.8) have been prepared through traditional solid-state sintering method. X-ray diffraction reveals a single-phase-layered perovskite structure for all compositions with shrinkage of the unit cell of SBN. The plate-like morphology revealed from SEM is symbolic of the characteristic Aurivillius phase of ceramics. Shifting of Raman phonon modes indicates the reduced rattling space of NbO_6 octahedral with an increase in Gd concentration. The dielectric properties of all compositions are studied as a function of temperature (RT–500 °C) over the frequency range (50 Hz to 1 MHz). Softening the lowest frequency mode with increasing x in SBGN shows the transition from ferroelectric to paraelectric at room temperature (RT). The flattening of dielectric permittivity and low dielectric loss is observed in SBN and gadolinium-modified SBN (SBGN) ceramic samples at RT. The phase transition becomes diffused and transition temperature gets shifted from 430 to 330 °C with an increase in gadolinium concentration at higher frequencies. The increase in broadness with an increase in frequency suggests that the presentation materials are of ferroelectric relaxor type. The degree of relaxor behavior (γ) increases from 1.05 for $x = 0.0$ to 1.57 for $x = 0.8$. The relaxor behavior along with diffuseness was noticed in the fabricated ceramics.

Address correspondence to E-mail: kiran.nischal@gmail.com

1 Introduction

SrBi₂Nb₂O₉ (SBN) has been regarded as a promising ferroelectric material due to the attributes of low dielectric constant, high mechanical quality factor, low electromechanical coupling coefficient, and an excellent electro-optic property. At present, bismuth-layered structure ferroelectrics (BLSFs) such as SrBi₂Nb₂O₉ (SBN) and SrBi₂Ta₂O₉ (SBT) are under good investigation as they have the most promising energy storage applications such as non-volatile random-access memories (NVRAM), sensors, actuators, fine tolerance oscillators, and high-capacitance capacitors [1–10]. When compared to non-layered ferroelectric Pb(Zr,Ti)O₃ (PZT), the layered ferroelectric SBN has several advantages such as fatigue-free, lead-free, minimum operating voltages, a high mechanical quality factor, and low-temperature coefficient of resonance frequency [11, 12]. SBN material of (Bi₂O₂)²⁺ interleaved with pseudo-perovskite blocks (A_{n-1}B_nO_{3n+1})²⁺ is sensitive to doping with various elements [13] and the bismuth layer influences the structural, electrical, and ferroelectric properties of the materials [14]. Sintering conditions and doping at different sites will lead to a change in the physical properties of the materials. As per our literature survey, rare earth group elements (or) lanthanides with incomplete 4f shell-doped interleaved structures find important technical applications in the field of electronics and optoelectronics. The studies based on perovskite-structured materials such as RMnO (R = Y, Dy, Ho, Tb, Yb, etc.) have exhibited multiferroic properties [15–19]. Lanthanides-doped SBN compound demonstrated a rise in the dielectric loss due to the annihilation of bismuth during the sintering process. Because of this, it is desirable to dope SBN with rare earth ions [20–22]. Hence, we have attempted to investigate the properties of SBN doped with gadolinium at Bi-site. In the present study, sintering conditions in the processing of SBN and gadolinium-doped SBN have been established and studied the effect of gadolinium on the structure, microstructure, and dielectric properties.

2 Experimental

Traditional solid-state sintering method was used to prepare the ceramic compositions, SrBi₂Nb₂O₉ (SBN), SrBi_{1.6}Gd_{0.4}Nb₂O₉ (SB_{0.4}GN), SrBi_{1.4}Gd_{0.6}Nb₂O₉

(SB_{0.6}GN), and SrBi_{1.2}Gd_{0.8}Nb₂O₉ (SB_{0.8}GN), using high pure powders of oxides and carbonate. The powders upon mixing were subjected to calcination at 800 °C for 2 h twice to enhance the homogeneity of the materials. The calcined materials were sintered in the temperature range of 1120 °C to 1150 °C. Either side of the pellet was electroplated using silver paste and was cured at 600 °C for 15 min. X-ray diffraction data were collected for these samples using CuKα radiation in the range (10° ≤ 2θ ≤ 90°). Scanning electron microscope (SEM) measurements are performed using VEGA3 TESCAN. Fourier transform infrared (FTIR) spectra of samples using KBr were recorded between 3500 and 400 cm⁻¹ using YLS-QC-WQP-004. The Raman spectra were recorded by Raman microscope using 785 nm solid-state laser beams. Dielectric measurements were carried out in the temperature and frequency range (RT–500 °C) and (50 Hz to 1 MHz), respectively, using an HP4284A impedance analyzer.

3 Results and discussion

3.1 Density

The optimum value of sintering temperature to obtain maximum sintered density has been achieved from density versus composition response, over a wide range of temperature (1120 to 1150 °C) as shown in Fig. 1 from Archimedes water

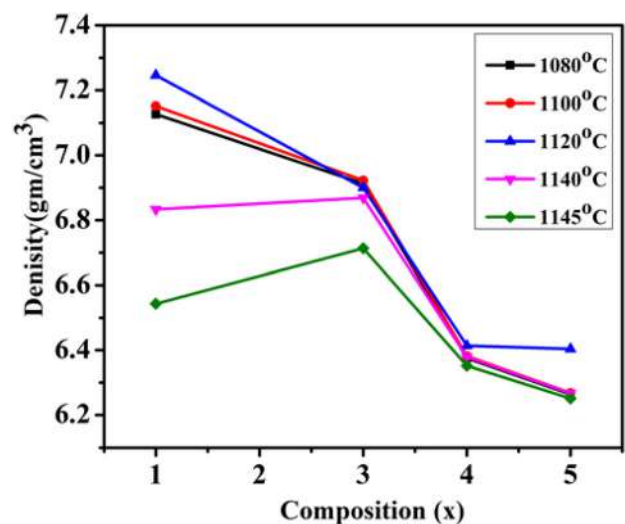


Fig. 1 Density versus composition response over the wide sintering temperature range in SrBi_{2-x}Gd_xNb₂O₉ (x = 0.0, 0.4, 0.6, and 0.8) ceramic compositions

displacement method (TTB15) by using Archimedes principle [23] with water as immersion liquid with its density $\rho_0 = 1 \text{ g/cm}^3$ and the expression for the determination of experimental density is

$$\rho = \frac{W_{\text{air}}}{W_{\text{air}} - W_{\text{water}}} \rho_0 \text{ g/cm}^3 \quad (1)$$

where W_{air} = weight of the prepared sample in the air and W_{water} = weight of the prepared sample when it is immersed in water. The maximum density for the studied samples has been obtained at 1120 °C for 2 h.

The theoretical density (ρ_T) was calculated from the X-ray diffraction patterns applying the formula:

$$\rho_T = \frac{N_f \times N}{N_V \times V} \text{ g/cm}^3 \quad (2)$$

where N_f is the number of formula units, N is the molecular weight of the compound, N_V is the Avogadro number, and V is the cell volume of the sample. The density percentage ($\rho\%$) after sintering was carried out using the following formula:

$$\rho(\%) = \frac{\rho_E}{\rho_T} \times 100 \quad (3)$$

where ρ_E is the experimental density g/cm^3 and ρ_T is the theoretical density in g/cm^3 of the ceramic sample.

3.2 X-ray diffraction analysis

X-ray diffraction pattern for $\text{SrBi}_{2-x}\text{Gd}_x\text{Nb}_2\text{O}_9$ compositions (x is varying from 0.4 to 0.8 in steps of 0.2) is shown in Fig. 2. A close examination of XRD spectra reveals a single-phase bismuth oxide layer-type structure with pseudo-perovskite units. The (1 1 5) peak shifted to a lower angle side as Gd^{3+} content increased from 0.4 to 0.8. It indicates Gd has successfully diffused into SBN lattice [15] and also the expansion of the crystal lattice compared to pure SBN. Meanwhile, substituting Gd^{3+} ion for Bi^{3+} ion with smaller ionic radii (0.938 \AA) in SBN would release tensions between the perovskite units and the $(\text{Bi}_2\text{O}_2)^{2+}$ layers, altering the structural distortion of the Aurivilius structure [24, 25] However, for Gd content at $x = 0.8$, additional peaks related to Gd_2O_3 could be identified. Furthermore, the (1 1 5) is not split but asymmetric and broadened. The relative intensity of (1 1 5) plane was found to decrease for gadolinium-substituted compositions and the peak

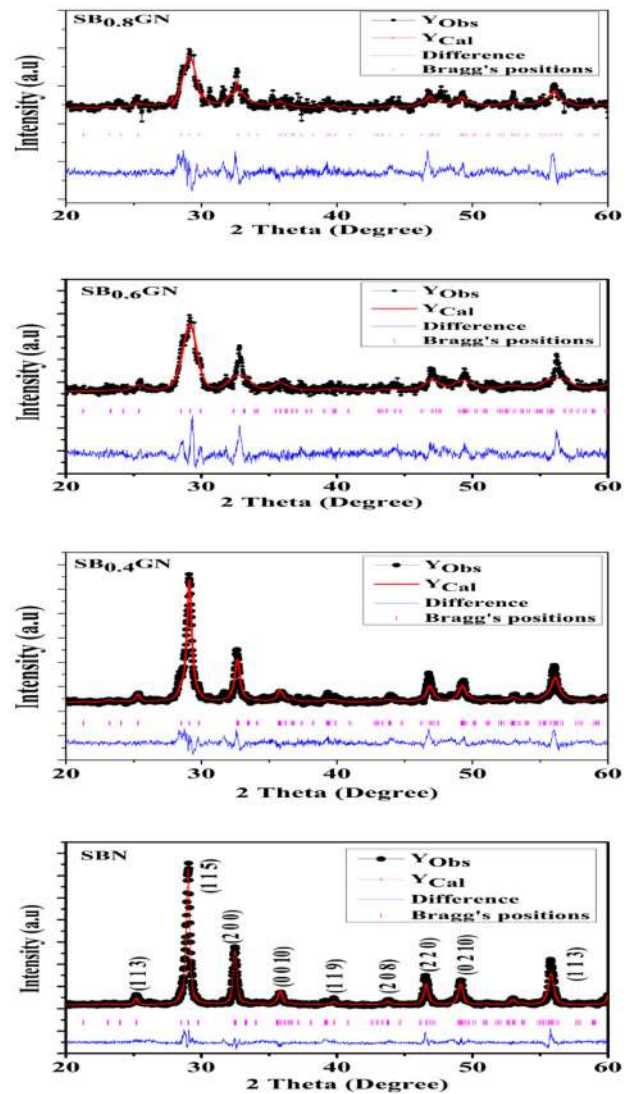


Fig. 2 Rietveld refinement of SBN and gadolinium-modified SBN ceramic powders

profiles became wider, as shown in Fig. 2. This indicates an increase in interplanar spacing (d) between the planes compared to SBN. The refinement parameters were tabulated in the table. 1, the obtained lattice parameters indicated that the crystal symmetry of all ceramic compositions is orthorhombic. It was noted that there was an insignificant change in the unit cell volume and orthorhombic distortion (b/a) with gadolinium substitution. The intensity variation in the peak may be due to an increase in internal stress in SBN particles resulting in an elastic compressive volume strain. This result indicates a significant relaxation of the unit cell at high doping levels, leading to a decrease in the cell volume. Generally, the complex arrangement of

Table 1 Rietveld refinement parameters for SBN and gadolinium-modified SBN ceramics

Compound	SBN	SB _{0.4} GN	SB _{0.6} GN	SB _{0.8} GN
Lattice parameter (Å)	5.5096; 5.1743; 25.0577	5.4633; 5.4984; 25.0583	5.5319; 5.4049 25.0669	5.4840; 5.4840; 25.0551
Cell Volume(Å ³)	761.726 (0.142)	752.754(0.699)	749.499	753.536
Orthorhombic distortion (b/a)	0.939	1.006	0.977	1.000
Atomic positions				
Sr				
x	– 10.02394	-0.05978	-0.06613	-0.07169
y	0.25683	0.27470	0.25427	0.24332
Z	0.00000	0.00000	0.00000	0.0000
Occupancy	0.734	0.941	1.012	0.999
Bi				
x	0.45801	0.47240	0.40443	0.39932
y	0.76618	0.74600	0.78075	0.70415
Z	0.19978	0.19858	0.19947	0.19710
Occupancy	0.769	0.532	0.767	0.564
Gd				
x	–	0.47240	0.50912	0.44529
y	–	0.74600	0.76198	0.75670
z	–	0.19858	0.19944	0.19912
Occupancy	–	0.958	0.990	0.953
Nb				
x	0.48312	0.48953	0.47187	0.47988
y	0.76423	0.76827	0.76247	0.75130
z	0.41261	0.41355	0.41566	0.41682
Occupancy	1.017	1.402	1.544	1.786
O				
x	0.72337	-0.3603	0.70716	0.67254
y	0.98276	0.94976	0.98101	0.97428
z	0.93120	0.93363	0.93299	0.93464
Occupancy	0.900	3.619	3.476	3.574
χ^2	1.77	1.16	1.13	1.88

cations in the ABO₃ structure shows changes in the vibrational spectra compared to the original. Therefore, in the present study, Raman scattering is considered to investigate the prepared samples.

The XRD patterns are used for Rietveld refinement using the Fullprof program [26]. In the Rietveld method, the difference between experimental and generated patterns is minimized by using user-selected parameters as given in Table 2. This model is developed using instrumental parameters and a known crystal structure as a starting point. This program refines the structural parameters (atomic positions, occupancies, and lattice parameters), instrumental parameters (background, peak profile parameters (u, v, w), and error correction parameters (zero shift) and asymmetric factors. This program

uses the pseudo-Voigt function to fit the experimental dataset. Refinement is carried out by considering the stoichiometry for all the concentrations studied. Figure 2 shows the Reitveld refinement fit of the SBN and gadolinium-modified SBN and they match well with the experimental XRD profile. Figure 3 represents the orthorhombic structure of SBN and gadolinium-modified SBN by Rietveld parameters. The obtained refinement parameters for the studied ceramics such as crystal lattice parameters, cell volume, atomic positions, and occupancies along goodness parameters (χ^2) are tabulated in Table 1.

Table 2 Details of Rietveld refinement parameters for $\text{SrBi}_{2-x}\text{Gd}_x\text{Nb}_2\text{O}_9$ ($x = 0.0, 0.4, 0.6, \text{ and } 0.8$) compositions

Composition	SBN	$\text{SB}_{0.4}\text{GN}$	$\text{SB}_{0.6}\text{GN}$	$\text{SB}_{0.8}\text{GN}$
Wavelength (Å)	1.54186	1.54186	1.54186	1.54186
Step scan increment (2θ)	0.02	0.02	0.02	0.02
2θ range ($^\circ$)	20–60	20–60	20–60	20–60
Program	FULLPROF	FULLPROF	FULLPROF	FULLPROF
Caglioti parameters	$U = 0.17352$ $V = 0.01147$ $W = 0.04975$	$U = 0.31420$ $V = 0.61263$ $W = 0.10191$	$U = 2.25188$ $V = 0.43501$ $W = 0.58674$	$U = 1.77356$ $V = 0.21092$ $W = 0.02468$
No of reflections	40	40	40	40
No. of refined parameters	06	16	08	16
Space group	A 21 a m	A 21 a m	A 21 a m	A 21 a m
R_F	9.87	6.91	5.36	5.71
R_B	12.4	9.5	10.5	12.5
R_p	13.8	12.1	13.2	13.0
R_{wp}	17.7	15.2	16.7	18.9
R_{exp}	13.32	14.08	15.71	13.81

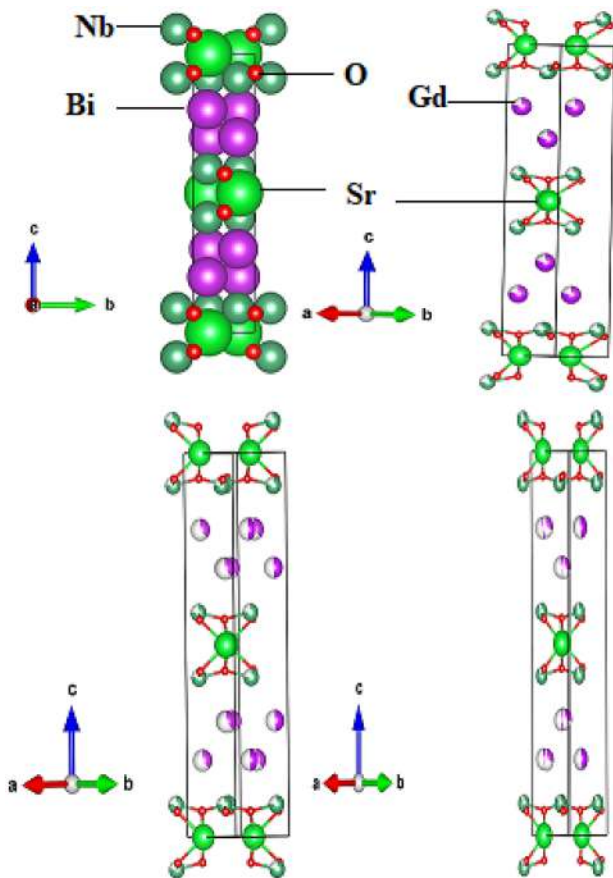


Fig. 3 Schematic representation of $\text{SrBi}_{2-x}\text{Gd}_x\text{Nb}_2\text{O}_9$ ($x = 0.0, 0.4, 0.6, \text{ and } 0.8$) packing diagrams generated by Rietveld parameters

3.3 Microstructure- SEM

Figure 4 depicts SEM micrographs containing grains of a random and unsystematic shape that indicate the polycrystalline nature of the samples sintered at 1120 °C. The plate-like morphologies observed in the undoped (SBN) sample are symbolic of the characteristic Aurivillius phase of ceramics [27, 28]. The microstructure of the prepared compounds is very much comparable to that of other compounds of the bismuth layer-structured materials family [29, 30]. The average grain size of the irregular-shaped grains has been calculated using Image J software, as given in Table 3. The grain size decreased on increasing Gd concentration in SBN may be due to the sintering temperature causing grain boundary movement retardation due to a lack of activation energy, which could prevent densification without grain growth while maintaining grain boundary diffusion. Grain growth mainly depends on the sintering temperature, the concentration of oxygen vacancies, and the rate of ion diffusion [31, 32]. In addition, an optimized sintering temperature would result in the minimization of pores and therefore a reduction in grain size, which helps to suppress grain growth [33]. Further, the microstructural characteristics may also be linked to matter transport phenomena between the grains during the sintering process [34]. High concentrations of gadolinium, i.e., more than 40 weight % may induce the formation of defects [35] in the structure, which is mainly due to possibility of occupancy onto other sites and high solid solubility nature. The

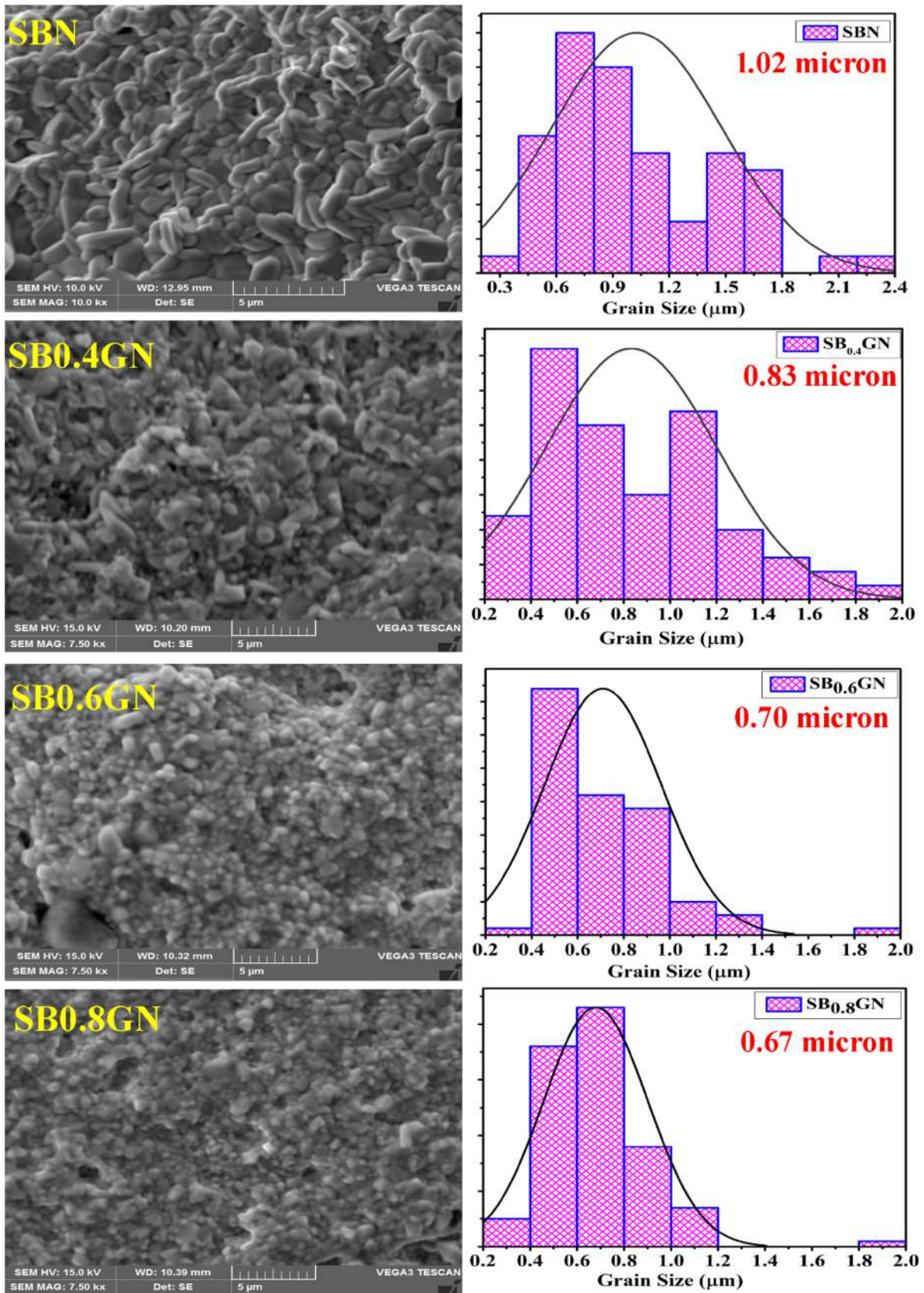


Fig. 4 SEM micrographs of SBN and gadolinium-doped $\text{SrBi}_{2-x}\text{Gd}_x\text{Nb}_2\text{O}_9$ ($x = 0.4, 0.6, \text{ and } 0.8$) ceramics

Table 3 Values of density, grain size, and porosity of SBN and gadolinium-substituted SBN

Composition	$\rho_E(\text{gm/cm}^3)$	$\rho_T(\text{gm/cm}^3)$	Relative density	Grain size (μm)	Porosity (%)
SBN	7.246	7.641	95	1.02	0.051
SB _{0.4} GN	6.900	7.074	97	0.83	0.024
SB _{0.6} GN	6.414	6.955	92	0.70	0.077
SB _{0.8} GN	6.404	6.962	92	0.67	0.080

porosity of the prepared samples was calculated from Eq. (4).

$$\text{Porosity} = 1 - \frac{\rho_E}{\rho_T} \tag{4}$$

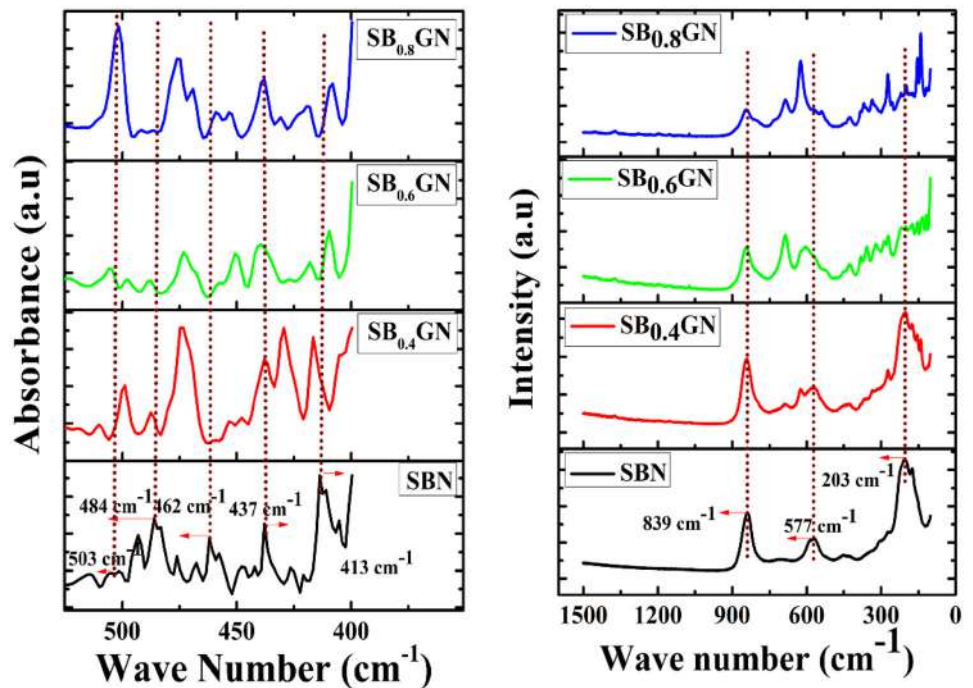
3.4 FTIR and Raman studies

FTIR and Raman spectra of the powders of SBN and SBGN calcined at 800 °C, as shown in Fig. 5. FTIR absorbance peaks were observed at 413 cm⁻¹, 437 cm⁻¹, 462 cm⁻¹, 484 cm⁻¹, and 503 cm⁻¹. The aforesaid IR peaks are inconsistent with earlier reported data [35]. The vibrational bands from 413 to 462 cm⁻¹ corresponding to the Nb–O bending vibration [36] and mode at 503 cm⁻¹ that can be assigned to Nb–O stretching vibration of NbO₆ octahedra are shown in Fig. 5a. Thus, the vibrational bands (437 cm⁻¹, 462 cm⁻¹, and 484 cm⁻¹) are identified shifting toward the lower wavenumber side in gadolinium-doped SBN, indicating that the

interatomic force constant between the Nb–O band is decreased. The observed shift of vibrational band (413 cm⁻¹ and 503 cm⁻¹) to the higher wavenumber side in SBGN ceramics can be attributed to a change in the bond strength and the atomic force constant due to the higher mass of Bi atoms to that of Gd, as shown in Fig. 5a [37–41].

Raman spectroscopy is a very effective and sensitive tool for identifying the phase purity of multi-component oxide material. Raman spectra obtained at room temperature on SBN and SBGN calcined powders are shown in Fig. 5b. The well-defined phonon modes around 203 cm⁻¹, 577 cm⁻¹, and 839 cm⁻¹ were observed for SBN ceramic, which is in good agreement with the reported data [42–44]. The Raman mode observed at 839 cm⁻¹ was assigned to symmetrical stretching of the NbO₆ octahedron and the modes at 203 cm⁻¹ and 577 cm⁻¹ to the rotation or inclination of NbO₆ octahedra [45]. When Gd was introduced into SBN, a significant shift in phonon modes was observed, especially above $x > 0.4$. It has

Fig. 5 FTIR and RAMAN spectra of SrBi_{2-x}Gd_xNb₂O₉ ($x = 0.0, 0.4, 0.6,$ and 0.8) ceramic powders



been observed that the phonon modes shift to a higher frequency side with the increase in Gd-doping concentration at the Bi-site of SBN. The NbO_6 octahedral linked to the Bi layer can shrink through the substitution of gadolinium at the bismuth site leading to an increase in the binding energy of NbO_6 , thereby resulting in a stronger bond and increased oscillation frequency for the modes at 203 cm^{-1} , 577 cm^{-1} , and 839 cm^{-1} . The structural distortion with increasing dopant concentration as observed in XRD has produced a shift in Raman peaks.

3.5 Dielectric studies

Figure 6a, b shows the dielectric constant (ϵ') and dielectric loss ($\tan\delta$) against frequency for SBN and gadolinium-doped SBN samples, at room temperature (RT). The observed high dielectric constant and $\tan\delta$ values for SBN could be interpreted as an extrinsic mechanism, which was assumed to result from the sample's microstructure such as an interface or interfacial effects [46]. As reported by Gerson et al., the increased porous presentation in a solid dielectric (porous ceramics) may reduce dielectric strength as it influences electrical breakdown [47], evident from Fig. 6a. Further, it was found that with an increase in gadolinium concentration in SBN, dielectric constant and $\tan\delta$ values were decreased, as mentioned in Table 4. The dielectric loss of the undoped (SBN) ceramic is many times higher than that of the doped ceramics when measured at RT (Table 4). A decrease in dielectric constant can be ascribed to the presence of Gd^{3+} ions in SBN, which is similar to the reports

Table 4 Dielectric properties of $\text{SrBi}_{2-x}\text{Gd}_x\text{Nb}_2\text{O}_9$ ($x = 0.0, 0.4, 0.6,$ and 0.8) specimens

Composition	T_c ($^\circ\text{C}$)	ϵ' (RT)	$\epsilon'(T_c)$	$\tan\delta$ (RT)
SBN	430	235	598	3.354
$\text{SB}_{0.4}\text{GN}$	350	168	201	0.395
$\text{SB}_{0.6}\text{GN}$	340	146	95	0.277
$\text{SB}_{0.8}\text{GN}$	330	73	60	0.264

from the literature survey [48–50]. The flattening of dielectric permittivity and low dielectric loss was observed from the present study as concluded by Afqir et al., [51]. Fig. 7a–d) shows the variation of dielectric permittivity (ϵ') versus temperature (RT–500 $^\circ\text{C}$) at selected frequencies for SBN and Gd^{3+} ion-doped SBN materials. A transition from Ferroelectric to Para electric phase was observed in all the studied materials. In the case of relaxor ferroelectric materials, broadening of dielectric peaks can be seen with the temperature at different frequencies. The temperature-based extensive broadening was observed with increasing doping concentration as shown in Fig. 7c and d. The value of transition temperature (T_c) in SBN has been found at $430\text{ }^\circ\text{C}$, noticed to be in close agreement with the literature value [52, 53]. The transition temperatures (T_c) of the studied ceramics are found to lie in the temperature range of $430\text{--}330\text{ }^\circ\text{C}$. Predominantly, the transition temperature of ferroelectric materials depends on their polarizability. The lower transition temperature in Gd^{3+} ion substituted samples is may be due to the

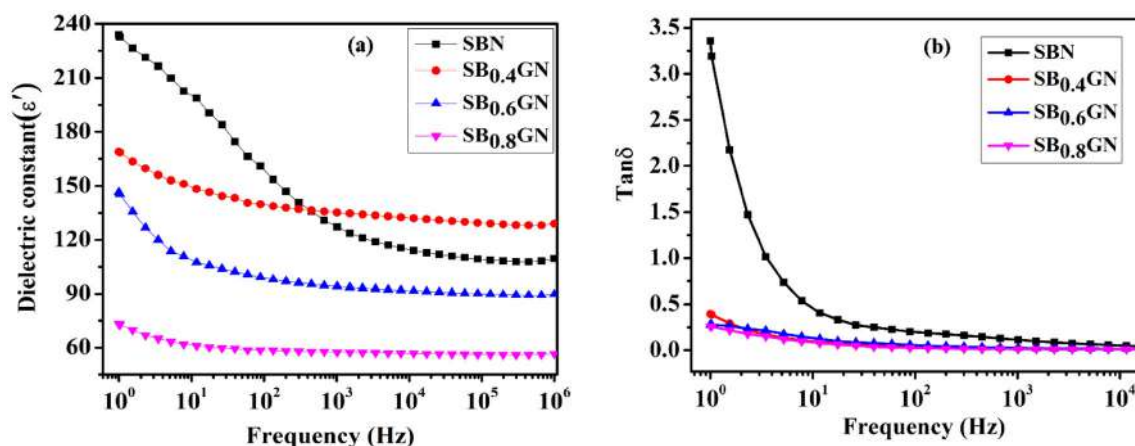


Fig. 6 Frequency dependence of the dielectric permittivity (ϵ') and dielectric loss ($\tan\delta$) at room temperature of Gd-doped $\text{SrBi}_2\text{Nb}_2\text{O}_9$ ceramics

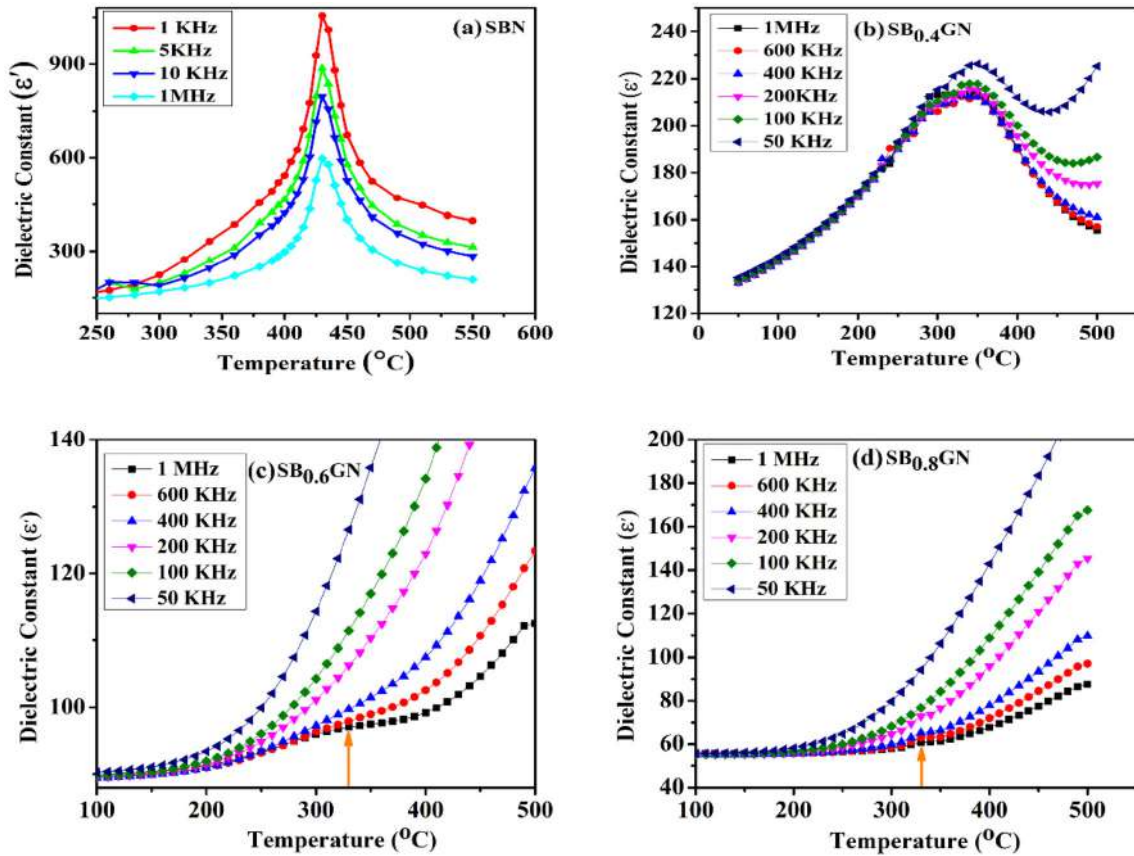


Fig. 7 Dielectric permittivity as a function of temperature at different frequencies of SBN and gadolinium-doped $\text{SrBi}_{2-x}\text{Gd}_x\text{Nb}_2\text{O}_9$ ($x = 0.4, 0.6,$ and 0.8) ceramic materials

size-dependent electronic polarization and decreased tetragonal strain in the sample [14, 54], as given in Table 3. The decrease in the Curie temperature with Gd^{3+} ion doping can also be due to changes in the Nb–O–Nb angles, which leads to a smaller rattle space for the Nb ions in the oxygen octahedron NbO_6 , which in turn reduces the ion shifts [55, 56]. The response of dielectric permittivity with the temperature at different frequencies showed a broad response. The broadness is found to increase with an increase in frequency. This suggests that the prepared materials are of relaxor type, which is in good agreement with earlier reports [57–59]. Hence, the studied relaxor ferroelectrics may find energy storage applications.

Figure 8a to d shows the typical dielectric constant versus frequency (100 Hz to 1 MHz) plots at different temperatures for all the ceramic samples. The variation of permittivity with an increase in frequency reveals the relaxor-type behavior of the samples. It indicates the typical thermally activated Debye

relaxation behavior in these frequency regions. The increase in dielectric permittivity at higher temperatures can be assigned to an increase in conductivity [48, 60] due to the rise in mobile charge carriers from the formation of oxygen vacancies due to the volatilization of bismuth during the sintering [61, 62]. The substitution of Gd^{3+} ion at Bi-site of SBN not only restrains the bismuth losses but also causes a decrease in conduction phenomenon, therefore dielectric permittivity decreased [63], as given in Table 4. Meanwhile, small polarization of Gd^{3+} ion in comparison with Bi^{3+} ion may also be the reason for small ϵ' [64].

Figure 9a–c shows the typical dielectric loss measured at different frequencies as a function of temperature. The dielectric loss measured at different temperatures as a function of frequency is shown in Fig. 9d–f. The decrease in dielectric loss with an increase in frequency in $\text{SB}_{0.4}\text{GN}$, $\text{SB}_{0.6}\text{GN}$, and $\text{SB}_{0.8}\text{GN}$ is due to the space charge and domain wall relaxation [65]. From Fig. 9a–c, we observed a

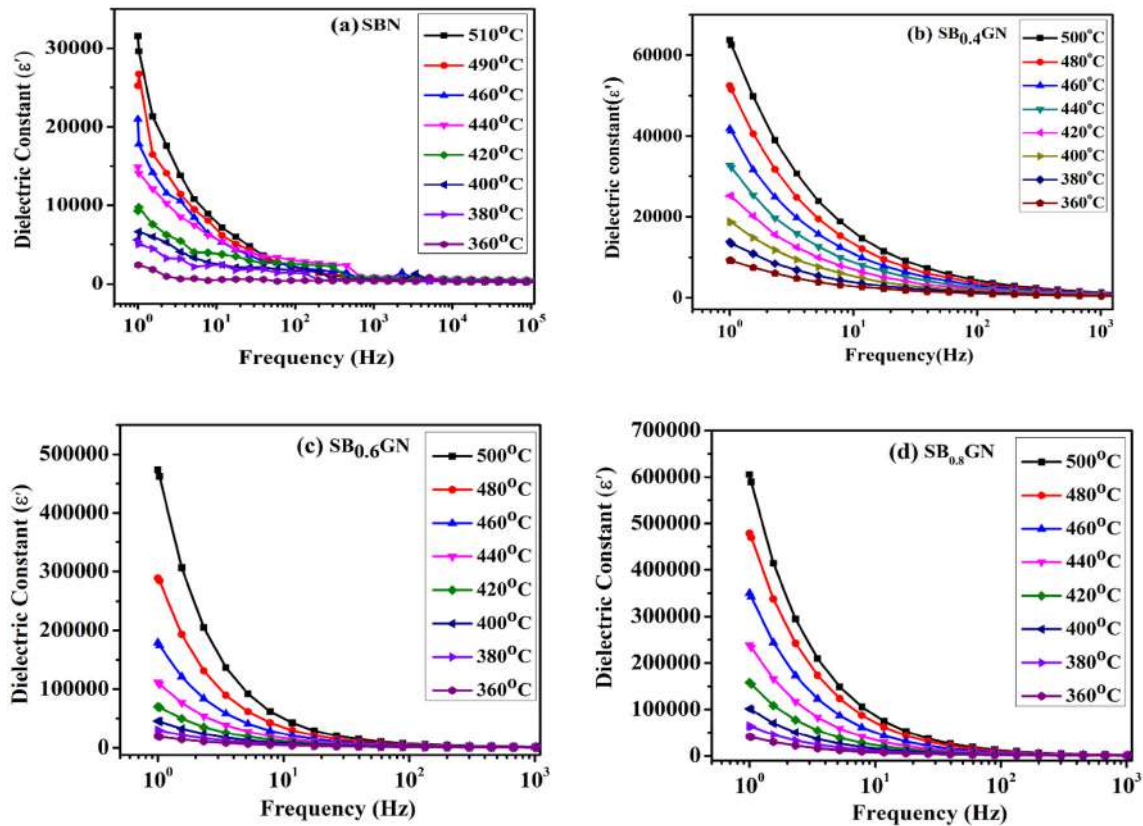


Fig. 8 Frequency dependence of dielectric permittivity at different temperatures of SBN and gadolinium-doped SBN ceramics

decrease in dielectric loss ($\tan \delta$) with an increase in frequency. It is also observed that the dielectric loss ($\tan \delta$) increases with an increase in doping concentration, which is similar to the dielectric behavior of the relaxor ferroelectrics. The appearance of a broadened dielectric loss peak as a function of temperature indicates a transition from one type of relaxation process to another occurring at a characteristic temperature and can be attributed to the combined effect of reorientation of thermally activated polarization when the temperature rises [66]. In addition, the high dielectric loss at higher temperatures is said to be induced by the thermally activated space charge contribution (Maxwell–Wagner type) [67]. As observed from Fig. 9d–f, the dielectric loss value increases with an increase in temperature for $\text{SB}_{0.4}\text{GN}$, $\text{SB}_{0.6}\text{GN}$, and $\text{SB}_{0.8}\text{GN}$ samples. Furthermore, the structural distortion observed from XRD analysis was realized from dielectric properties as a function of frequency. The dielectric constant was found to increase with the increase in dopant concentration.

3.6 Diffusivity parameter

The modified Curie–Weiss law is employed to understand diffuse phase transition and relaxation behavior in the material. The modified Curie–Weiss law was given in Eq. (5).

$$\frac{1}{\epsilon} - \frac{1}{\epsilon'_{\max}} = \frac{(T - T_m)\gamma}{C} \quad (5)$$

where ϵ'_{\max} is maximum permittivity at T_m , ϵ' is the permittivity, T is the temperature above T_m (in the paraelectric region), C is a constant, and γ is the diffuseness parameter representing the degree of dielectric relaxation ($1 \leq \gamma \leq 2$). For a normal ferroelectric, $\gamma = 1$. For a completely disordered ferroelectric, $\gamma = 2$ [68–70]. When $1 < \gamma < 2$, the material is called relaxor ferroelectric. Figure 10 shows the $\ln(1/\epsilon' - 1/\epsilon'_{\max})$ versus $\ln(T - T_m)$ plots of SBN and Gd-doped SBN samples at 1 MHz. The diffuseness parameter (γ) was found to be 1.28 in $\text{SB}_{0.4}\text{GN}$ [71]. This shows the diffuse nature of phase transition in $\text{SB}_{0.4}\text{GN}$. The diffuse phase transition (DPT) can mainly be due to the substitution of cation-host with

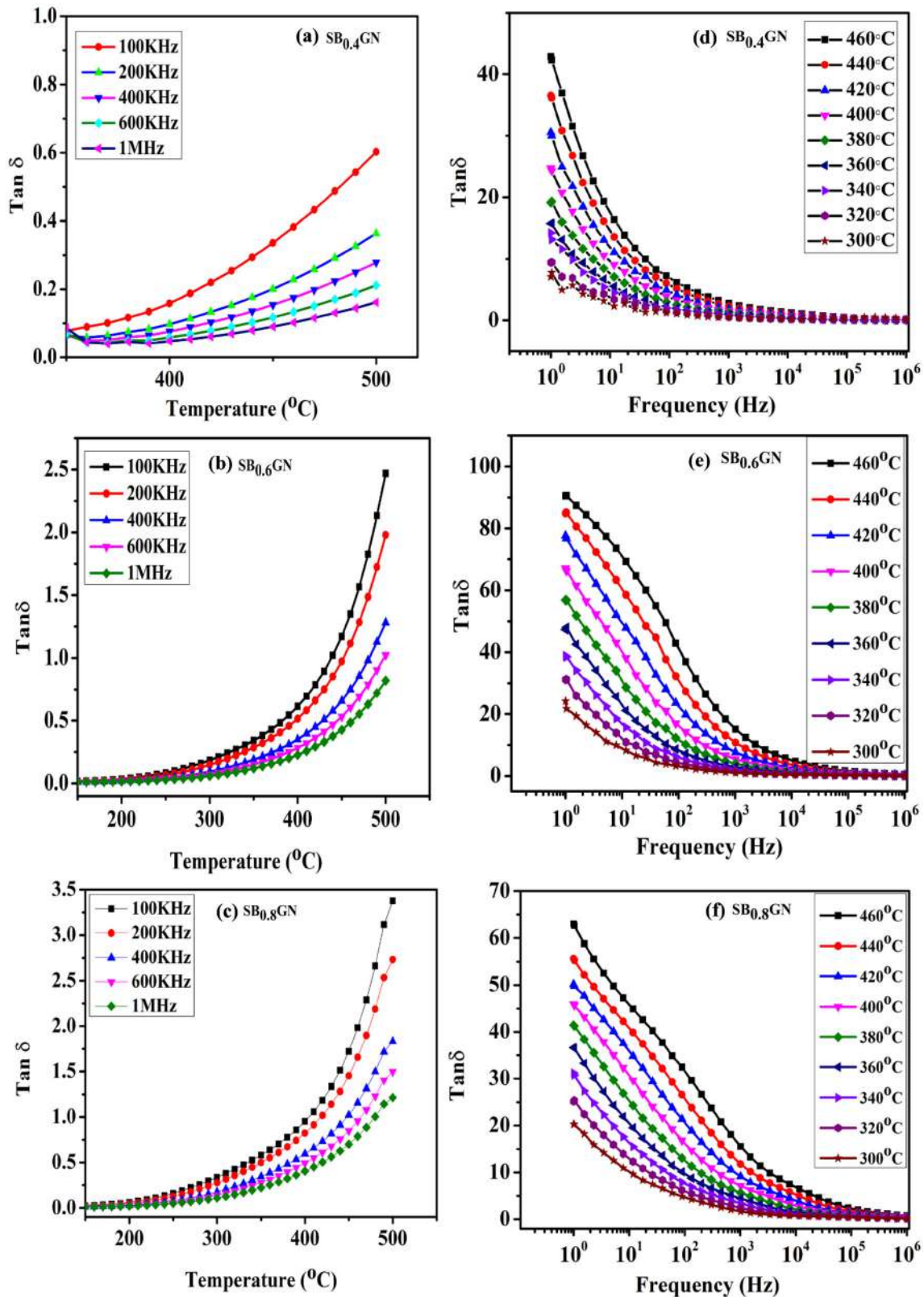


Fig. 9 a Dielectric loss versus temperature at different frequencies of gadolinium-doped $SrBi_{2-x}Gd_xNb_2O_9$ ($x = 0.4, 0.6, \text{ and } 0.8$) ceramic materials and b dielectric loss versus frequency at different temperatures of $SB_{0.4}GN$, $SB_{0.6}GN$, and $SB_{0.8}GN$ ceramic materials

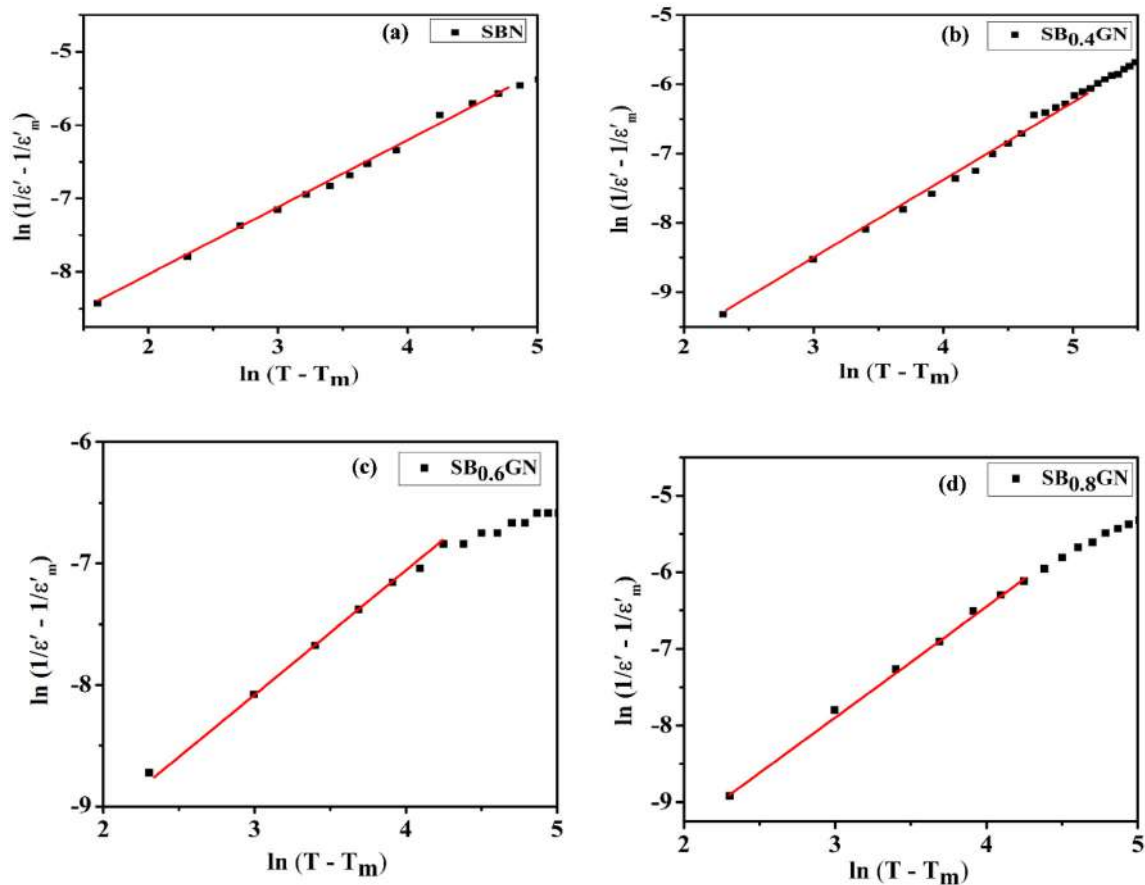


Fig. 10 $\ln(1/\epsilon' - 1/\epsilon'_m)$ versus $\ln(T - T_m)$ plots of SBN and SBGN ceramics at 1 MHz

Table 5 Variation of diffuseness parameter with gadolinium (Gd) content in SBN

Ceramic material	Gd content (weight %)	Diffuseness parameter (γ)
SBN	0.0	1.05
SB _{0.4} GN	0.4	1.28
SB _{0.6} GN	0.6	1.49
SB _{0.8} GN	0.8	1.57

some elements having different ionic radii [72, 73]. The γ values increased from 1.28 to 1.57 with an increase in gadolinium content implying the diffuseness behavior, as given in Table 5. The diffusion of Gd^{3+} ion into the $(\text{Bi}_2\text{O}_2)^{2+}$ slabs and hence resulting in distortion may be a possible reason for the diffuseness behavior in the present ceramic materials [74, 75]. The revision in the diffusivity parameter values can also be accorded to the structural distortion. The relaxor behavior along with diffuseness was noticed in the fabricated ceramics.

4 Conclusion

Polycrystalline $\text{SrBi}_{2-x}\text{Gd}_x\text{Nb}_2\text{O}_9$ ($x = 0.0, 0.4, 0.6,$ and 0.8) ceramic materials were prepared by the traditional solid-state sintering method. High dense, about 92–97%, ceramic samples are obtained by optimizing sintering conditions. X-ray diffraction analysis showed that single-phase-layered perovskite structures were obtained for all compositions with shrinkage of the unit cell of SBN with the incorporation of Gd^{3+} dopant having lone pair of electrons. The plate-like morphology revealed from SEM is symbolic of the characteristic Aurivillius phase of ceramics with an average grain size of 0.6–1.0 μm .

FTIR shows the distortion of NbO_6 octahedral with Gd doping. Substitution of gadolinium at Bi-site resulted in the reduction rattling space for NbO_6 octahedral giving a significant shift in the Raman mode corresponding to NbO_6 (203 cm^{-1} and 577 cm^{-1}) and soft mode disappeared at $x = 0.8$. The increased concentration of Gd in SBN decreased T_c from 430 to 330 °C. The dielectric constant versus temperature response at different frequencies showed a broad response, suggesting that the present samples are of ferroelectric relaxor type. The degree of relaxor behavior (γ) increased from 1.05 for $x = 0.0$ to 1.57 for $x = 0.8$, confirming that the materials belong to relaxor ferroelectrics ($\gamma = 1 \leq x \leq 2$).

Author contributions

All authors contributed to the study's conception and design. Material preparation, data collection, and analysis were performed by [SN], [JAK], and [BNR]. The first draft of the manuscript was written by [JNK], [BSBR], and [KSR], and all authors commented on previous versions of the manuscript. All authors read and approved the final manuscript.

Funding

The authors declare that no funds, grants, or other support was received during the preparation of this manuscript.

Declarations

Conflict of interest Authors have no potential conflicts of interest. The present research involved no human and/or animal participants. The authors have no relevant financial or non-financial interests to disclose.

Research Data Policy and Data Availability Statements The datasets generated during and/or analyzed during the current study are available from the corresponding author on reasonable request.

References

1. B.H. Park, B.S. Kang, S.D. Bu, T.W. Noh, J. Lee, W. Jo, *Nature* **401**(6754), 682 (1999)
2. J.S. Kim, S.S. Kim, *Appl. Phys. A* **81**, 1427 (2005)
3. III W. Kim, C.W. Ahn, *Appl. Phys. Lett.* **80**(21), 4006 (2002)
4. X.L. Zhong, J.B. Wang, M. Liao, L.Z. Sun, H.B. Shu, C.B. Tan, Y.C. Zhou, *Appl. Phys. Lett.* **90**, 102906 (2007)
5. Y. Shimakawa, Y. Kubo, Y. Tauchi, H. Asano, T. Kamiyama, F. Izumi, Z. Hiroi, *Appl. Phys. Lett.* **779**(17), 2791 (2000)
6. M.M. Kumar, Z.-G. Ye, *J. Appl. Phys.* **90**(2), 934 (2001)
7. T.Y. Kim, J.H. Lee, Y.J. Oh, M.R. Choi, H.R. Yoon, W. Jo, H.J. Nam, *J. Korean Phys. Soc.* **49**(9(7)), 595 (2006)
8. S.M. Jung, S.I. Yoo, Y.H. Kim, Y.T. Kim, S.K. Hong, *J. Korean Phys. Soc.* **49**(9(7)), 552 (2006)
9. B. Aurivillius, *Ark. Kemi* **1**, 449 (1951)
10. J.F. Scott, C.A.P. de Araujo, *Science* **246**(4936), 1400 (1989)
11. A. Ando, M. Kimura, Y. Sakabe, *Proceedings of the 11th international symposium on application of Ferroelectrics IEEE-UFC*, (1999) 303–306
12. A. Ando, M. kimura, Y. Sakabe, *Crystalline structure and piezoelectric properties of Bi layer structured compound $\text{SrBi}_2\text{Nb}_2\text{O}_9$* , *Extended Abstract of the 9th US-Japan seminar on Dielectric and piezoelectric ceramics*. (1999) 115–118
13. V. Srivastava, A.K. Jha, R.G. Mendiratta, *Mat. Lett.* **60**, 1469 (2006)
14. V. Srivastava, A.K. Jha, R.G. Mendiratta, *Physica B* **371/2**, 337 (2006)
15. M. Afqir, A. Tachafine, D. Fasquelle, M. Elaammani, J.-C. Carru, A. Zegzouti, M. Daoud, *Solid State Sci.* **73**, 51 (2017)
16. A. Rotaru, A.J. Miller, D.C. Arnold, F.D. Morrison, *Phil. Trans. R. Soc. A* **372**, 20120451 (2014)
17. G.A. Smolenskii, V.A. Bokov, *J. Appl. Phys.* **35**(3), 915 (1964)
18. T. Katsufuji, M. Masaki, A. Machida, M. Moritomo, K. Kato, E. Nishibori, M. Takata, M. Sakata, K. Ohoyama, K. Kitazawa, H. Takagi, *Phys. Rev. B* **66**, 134434 (2002)
19. A. Munoz, J.A. Alonso, M.J. Martinez-Lope, M.T. Casais, J.L. Martinez, M.T. Fernandez-Diaz, *Chem. Mater.* **13**, 1497 (2001)
20. M. Afqir, A. Tachafine, D. Fasquelle, M. Elaammani, J. Carru, A. Zegzouti, M. Daoud, *Process. Appl. Ceram.* **10**(3), 183 (2016)
21. M. Afqir, A. Tachafine, D. Fasquelle, M. Elaammani, A. Zegzouti, J.C. Carru, M. Daoud, *Moscow Univ. Phys. Bull.* **72**(2), 196 (2017)
22. M. Afqir, A. Tachafine, D. Fasquelle, M. Elaammani, J. Carru, A. Zegzouti, M. Daoud, *Sci. China Mater.* **59**, 921 (2016)
23. J.E. Shelby, *Introduction to Glass Science and Technology*, 2nd edn. (The Royal Society of Chemistry, London, 2015)

24. F. Rehman, H.-B. Jin, J.-B. Li, RSC Adv. **6**, 35102 (2016)
25. F. Rehman, L. Wang, H.-B. Jin, A. Bukhtiar, R. Zhang, Y. Zhao, J.-B. Li, J. Am. Ceram. Soc. **100**, 602 (2017)
26. J. Rodriguez-Carvajal, in: Fullprof suite program laboratoire Leon Brillouin (CEA-C-NRS), France, 2015.
27. Y. Wang, J. Wu, Z. Peng, Q. Chen, D. Xin, D. Xiao, J. Zhu, Appl. Phys. A **119**(1), 337 (2015)
28. A. Long, H. Fan, P. Ren, Pubs. Acs. Org. **9**, 5045 (2013)
29. A.M. Wang, J. F. Wang, Appl. Phys. Lett. **89**, 202905/1–3 (2006).
30. N.V. Prasad, G. Prasad, T. Bhimasankaram, S.V. Suryanarayana, G.S. Kumar, Bull. Mater. Sci. **24**, 487 (2001)
31. I.-Wei Chen, X.-H. Wang, Nature, **404**, 168–171 (2000).
32. Su. Hua, X. Tang, H. Zhang, Z. Zhong, J. Shen, J. Appl. Phys. **109**, 07A501-13 (2011)
33. F.T.Z. Tomaa, I.N. Eshaa, M. Al-Amina, M.N.I. Khanb, K.H. Mariaa, J. Ceram. Process. Res. **18**, 1–10 (2017)
34. P. Fang, H. Fan, Z. Xi, W. Chen, W. Long, X. Li, J. Allys Comd. **50**, 335–338 (2015)
35. G.H. Haertling, C.E. Land, J. Am. Ceramic Soc. **54**, 1 (1971)
36. S. Nagamani, J. Nitchal Kiran, B. Siva Basivi Reddy, B. Nageswara Rao, J. Anindhya Kiran, K. Sambasiva Rao, ECS J. Solid State Sci. Technol. **10**, 410–02 (2021)
37. M. Verma, A. Tanwar, K. Sreenivas, V. Gupta, Ferroelectrics **404**(1), 233 (2010)
38. Y.X. Li, G. Chen, H.J. Zhang, Z.H. Li, J.X. Sun, J. Solid State Chem. **181**(10), 2653 (2008)
39. M. Zhu, L. Sun, W.W. Li, W.L. Yu, Y.W. Li, Z.G. Hu, J.H. Chu, Mater. Res. Bull. **45**(11), 1654 (2010)
40. J.T. Last, Infrared-Absorption Studies on Barium Titanate and Related Materials. Phys. Rev. **105**(6), 1740–1750 (1957)
41. M. Afqir, A. Tachafine, D. Fasquelle, M. Elaammani, J.-C. Carru, A. Zegzouti, M. Daoud, Chin. J. Phys. **56**(3), 1158 (2018)
42. M. Verma, K. Sreenivas, V. Gupta, J. Appl. Phys. **105**(2), 024511 (2009)
43. L. Sun, C. Feng, L. Chen, S. Huang, J. Appl. Phys. **101**(8), 084102 (2007)
44. S. Kojima, I. Saitoh, T. Yamamoto, Proceedings of the 11th IEEE International Symposium on Applications of Ferroelectrics, 1998 P. 471
45. H. Hao, H.X. Liu, M.H. Cao, X.M. Min, S.X. Ouyang, Appl. Phys. A **85**(1), 69 (2006)
46. S. Khasa, P. Singh, S. Sanghi, N. Singh, A. Agarwal, J. Integr. Sci. Technol. **2**, 13 (2014)
47. R. Gerson, T.C. Marshall, J. Appl. Phys. **30**(11), 1650–1653 (1959)
48. J. Wang, G. Rong, N. Li, C. Li, Q. Jiang, H. Cheng, Russ. J. Appl. Chem. **88**(3), 533 (2015)
49. M. Kallel, I. Kriaa, H. Khemakhem, Ceram. Int. **42**(1), 1379 (2016)
50. N. Haddadou, J. Belhadi, B. Manoun, K. Taibi, B. Carcan, M. El Marssi, A. Lahmar, J. Mater. Sci.: Mater. Electron. **29**, 16144 (2018)
51. M. Afqir, A. Tachafine, D. Fasquelle, M. Elaammani, J.-C. Carru, A. Zegzouti, M. Daoud, J. Mater. Sci. Mater. Electron. **29**(2), 1289 (2017)
52. V. Shrivastava, A.K. Jha, R.G. Mendiratta, Physica B **371**(2), 337 (2006)
53. Y. Shimakawa, H. Imai, H. Kimura, S. Kimura, Y. Kubo, E. Nishibori, M. Takata, M. Sakata, K. Kato, Z. Hiroi, Phys. Rev. B. **66**(14), 144110 (2002)
54. I. Coondoo, A.K. Jha, S.K. Aggarwal, J. Eur. Ceram. Soc. **27**(1), 253 (2007)
55. S. Huang, C. Feng, L. Chen, X. Wen, Solid State Commun. **133**(6), 375 (2005)
56. L. Sun, J. Hao Chu, P. Xiong Yang, F. Yu Yue, Y. Wei Li, C. De Feng, C. Liang Mao, Trans. Nonferrous Met. Soc. China, **19**(6), 1459 (2009)
57. A.A. Bokov, Z.-G. Ye, J. Adv. Dielectr. **2**(2), 1241010 (2012)
58. M. Varma, K. Sreenivas, V. Gupta, J. Appl. Phys. **105**, 024511 (2009)
59. L. Sun, C. Feng, L. Chen, S. Huang, J. Am. Ceram. Soc. **90**(1), 322 (2007)
60. P. Goeland, K.L. Yadav, Physica B **382**(1–2), 245 (2006)
61. Y. Wu, C. Nguyen, S. Seraj, M.J. Forbess, S.J. Limmer, T. Chou, G. Cao, J. Am. Ceram. Soc. **84**(12), 2882 (2001)
62. A. Khokhar, P.K. Goyal, O.P. Thakur, K. Sreenivas, Ceram. Int. **41**(3), 4189 (2015)
63. M. Ajmal, M.U. Islam, G.A. Ashraf, M.A. Nazir, M.I. Ghouri, Physica B (in Press)
64. M. Adamczyk, Z. Ujma, M. Pawelczyk, J. Mater. Sci. **41**(16), 5317 (2006)
65. I. Coondoo, A.K. Jha, S.K. Aggarwal, Ceram. Int. **33**(1), 41 (2007)
66. K. Li, X.L. Zhu, X.Q. Liu, X.M. Chen, Appl. Phys. Lett. **101**(4), 042906 (2012)
67. Y. Zhang, H. Sunn, W. Chen, Ceram. Int. **41**(7), 8520 (2015)
68. G.A. Smolenskii, A.I. Agranovskaya, Inst. Semi-Conductors **28**, 1380 (1958)
69. P. Victor, R. Ranjith, S.B. Krupanidhi, J. Appl. Phys. **94**(12), 7702 (2003)
70. A.R. Bowen, D.P. Almond, Mat. Sci. Technol. **22**(6), 719 (2006)
71. A. Dhak, P. Dhak, P. Pramanik, J. Electroceram. **27**(2), 56 (2011)
72. Y. Noguchi, M. Miyayama, K. Oikawa, T. Kamiyama, M. Osada, M. Kakihana, Jpn. J. Appl. Phys. **41**(11S), 7062 (2002)

73. E.C. Subbarao, J. Phys. Chem. Solids. **23**(6), 665 (1962)
74. C. Long, H. Fan, P. Ren, Struct. Inorg. Chem. **52**(9), 5045 (2013)
75. C. Long, Q. Chang, Y. Wu, W. He, Y. Li, H. Fan, J. Mater. Chem. C. **3**(34), 8852–8886 (2015)

Publisher's Note Springer Nature remains neutral with regard to jurisdictional claims in published maps and institutional affiliations.